SIMULATION METHODOLOGY ON ANALYZING CLAMPING MODE FOR SINGLE PROTON EXCHANGE MEMBRANE FUEL CELL

C.-Y. Wen [*] **H.-T. Chang** [**] **T.-W. Luo** [***]

Department of Aeronautics and Astronautics
National Cheng Kung University
Tainan City, Taiwan 70101, R.O.C.

ABSTRACT

In proton exchange membrane fuel cells (PEMFCs), a low interfacial pressure between the bipolar plates and the membrane exchange assembly (MEA) results in a high contact resistance. Conversely, an excessive interfacial pressure reduces the porosity of the gas diffusion layer (GDLs) and may damage the proton exchange membrane (PEM). Consequently, the performance of a PEMFC is critically dependent upon the clamping method. Accordingly, this study emphasizes the development of a numerical methodology for analyzing clamping of a PEMFC and constructs a detailed three-dimensional (3D) full-scale finite element (FE) model of a PEMFC with the traditional and most popular point-load design as an example. The numerical method is first validated by experiments. A series of simulations are then performed on the example cases (*i.e.* 2-bolt, 4-bolt or 6-bolt) to analyze their behaviors on the contact pressure between the bipolar plates and the MEA and the corresponding effects on the GDL porosity and the contact resistance, under the constraints that the membrane and gaskets remain within their respective elastic limits and the porosity of the GDL has a value higher than 0.5. Overall, to complete the analysis procedures proposed in this paper, the results show that the six-bolt clamping mode with a tightening torque of 16 N-m achieves a uniform pressure distribution and a high interfacial pressure, and therefore represents the optimal clamping mode for the performed example cases.

Keywords: Proton exchange membrane fuel cell, Clamping method, Three-dimensional simulation, Interfacial contact pressure.

1. INTRODUCTION

Polymer Electrolyte Membrane fuel cells, also known as Proton Exchange Membrane fuel cells (PEMFC), transform the chemical energy released by the reaction between hydrogen and oxygen to electrical energy. PEMFCs are characterized by a high power density, a low temperature operation, a virtually instantaneous recharging capability, and mechanical robustness. Furthermore, PEMFCs produce only water as a byproduct, and thus they represent an ideal solution for the development of eco-friendly transport applications and stationary or portable fuel cell systems. As shown in Fig. 1, a single PEMFC comprises a membrane exchange assembly (MEA) composed of a polymer membrane sandwiched between two gas diffusion layers (GDLs) coated with a catalyst material, positioned in turn between two bipolar plates housing flow channels for the anode and cathode gases (*i.e.* hydrogen and oxygen, respectively). In a practical application, multiple PEMFCs are stacked together to achieve the specified output power and voltage. In general, the fuel cell clamping can be categorized into three types: Point- load design, line-load design and surface-load design [1].

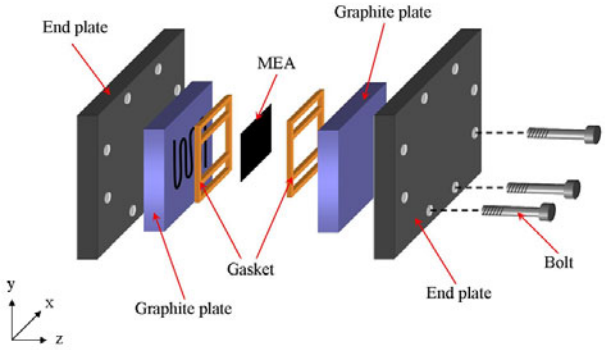


Fig. 1 Assembly break-down of PEMFC

The performance of a single PEMFC is critically dependent upon the interfacial contact pressure between the bipolar plate and the GDL. An insufficient clamping force results in a low interfacial contact pressure, which in turn produces a high contact resistance between the bipolar plate and the GDL and therefore reduces the fuel cell efficiency [1-3]. Conversely, an excessive clamping force not only reduces the porosity of the GDL, thereby inhibiting the proton exchange

[*] Professor, corresponding author [**] Postdoctoral researcher [***] Graduate student

DOI : 10.1017/jmech.2011.57
Copyright © 2011 The Society of Theoretical and Applied Mechanics, R.O.C.
https://doi.org/10.1017/jmech.2011.57 Published online by Cambridge University Press

mechanism, but may even cause structural damage to the components within the fuel cell, rendering it inoperable. Consequently, in optimizing the performance of a PEMFC, a careful specification of the clamping force is essential [1].

In a PEMFC, the GDLs play an essential role in diffusing the anode and cathode gases, discharging the liquid water byproduct, and conducting the electricity produced by the reaction between the fuel and the oxidant. In general, for a compressed GDL, the thermal contact resistance between GDL and bipolar plate was decreased nonlinearly with increasing compression pressure [4]. Variations in GDL thickness and porosity due to compression affect the local transport phenomena since gas permeability, electric conductivity and electric and thermal contact resistances at the interfaces with neighboring components are all dependent on compression [4,5]. Example of the current density distribution at the GDL / catalyst layer interface was increases with an increasing porosity or a decreasing GDL thickness [5]. Of all the components within the PEMFC, *e.g.* the membrane, the bipolar plates and the end plates, the GDL experiences the greatest deformation under the effects of the clamping force. This deformation has a significant effect upon the pore size of the GDL (and hence on its permeability characteristics), and therefore has a direct impact upon the power density and efficiency of the fuel cell. It has been reported that this effect is particularly pronounced in PEMFCs containing inter-digitated or serpentine flow channels [6,7]. In practice, the output characteristics of a PEMFC are dependent not only on the magnitude of the clamping force, but also on the uniformity of the resulting interfacial pressure distribution between the bipolar plates and the GDLs. Thus, the literature contains various proposals for stacking designs aimed at achieving a uniform pressure distribution [8-10].

With recent advances in computer performance, the CAE approach applies to the research of PEMFC can be useful in predicting the effects of various parameters on the performance of PEMFC. Further, it is possible to achieve a substantial reduction in development and testing time which relies mainly on the means of expensive and time consuming experimental testing. Therefore, various researchers have performed numerical simulations based on simplified 3D models [11] or 2D models [12,13] to investigate the contact pressure between the bipolar plates and the GDLs in a PEMFC following the clamping process, and to examine the corresponding effects upon the fuel cell performance. Furthermore, some researchers have used simple 2D models of the bipolar plates and the MEA to predict the effects of the assembly pressure on the mechanical behavior of the PEM in the fuel cell [14-17].

However, whilst computationally convenient, the use of simplified models inevitably limits the precision and reliability of the numerical results. Accordingly, the current study constructs a full-scale finite element model of a PEMFC utilizing Altair HyperMesh software and then performs ABAQUS simulations to predict the clamping performance. The traditional and most popular point-load design with the assembly of several pairs of bolts and nuts is adopted to demonstrate the analysis methodology. To ensure the accuracy of the simulation results, the model is constructed entirely of 3D elements and includes all the major components within a typical PEMFC, namely the end plates, the bipolar plates, the gaskets, the GDLs and the membrane. The validity of the numerical model is confirmed by comparing the ABAQUS simulation results obtained for the mean interfacial pressure between the GDL and the bipolar plate under various clamping modes with the experimental results obtained using a physical mock-up of the PEMFC incorporating a pressure-sensitive film. A series of simulations is then performed to examine the effects of the clamping mode (*i.e.* the number of bolts and the clamping torque) on the fundamental properties of the PEMFC, namely the interfacial contact pressure between the bipolar plate and the GDL, the deformation of the bipolar plate, the deformation of the GDL, the mean contact pressure between the bipolar plate and the GDL, the contact resistance between the bipolar plate and the GDL, and the porosity of the GDL. The proposed systematical approach can also be applied to the analyses and designs of other clamping methods, including line-load design and surface-load design.

2. OVERVIEW OF STUDY OBJECTIVES

The magnitude of the fuel cell voltage induced by the simultaneous reaction and reduction processes on the anode side and cathode side, respectively, depends on many parameters, including the cell temperature, the contact pressure between the bipolar plates and the GDL, the relative humidity, and so forth. However, as yet, the literature contains no complete closed-form analytical models for examining the respective effects of each of these parameters on the fuel cell performance.

Accordingly, the present study constructs and verifies a full-scale 3D model of a PEMFC in order to analyze the clamping performance of the fuel cell without the need for expensive and time-consuming experimentation. In general, the model provides a powerful tool for examining the mechanical behavior of the various components within the fuel cell and for understanding how this behavior affects the electrical characteristics of the cell. In this particular study, the model is used as the basis for a systematic procedure comprising both simulation processes and quantitative analytical techniques to analyze the clamping mode of the PEMFC. As shown in Fig. 2, the analysis procedure commences by certifying the PEMFC model. As discussed later in Section 5, this is achieved by comparing the simulation results obtained for the mean interfacial pressure between the GDL and the bipolar plate with the experimental results obtained using a pressure-sensitive film. Having confirmed the validity of the 3D PEMFC model, an analysis routine is performed to determine the number of clamping bolts (*i.e.* 2, 4 or 6) which maximizes the uniformity of the

https://doi.org/10.1017/jmech.2011.57 Published online by Cambridge University Press

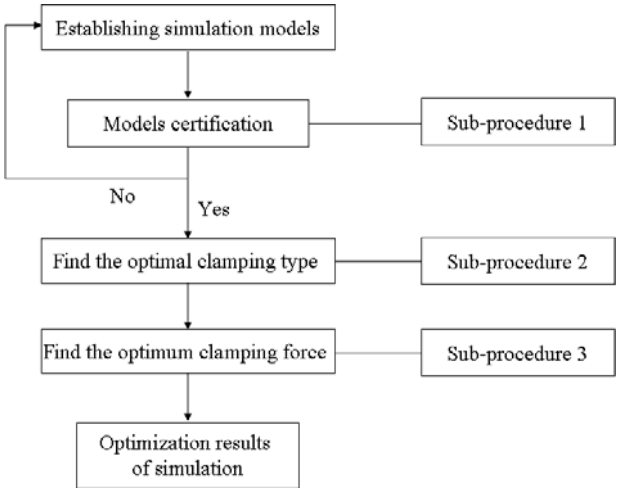
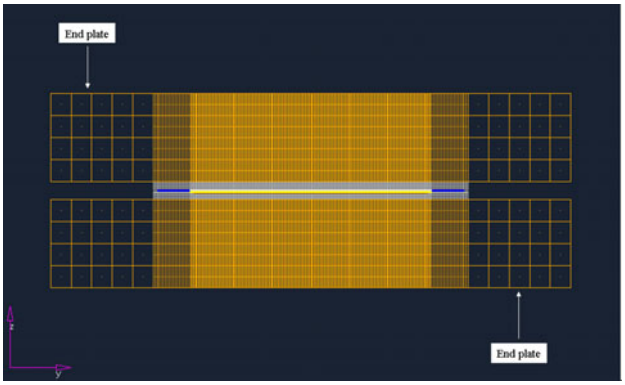


Fig. 2 A simplified flow chart showing overall structure of analysis procedure of methodology

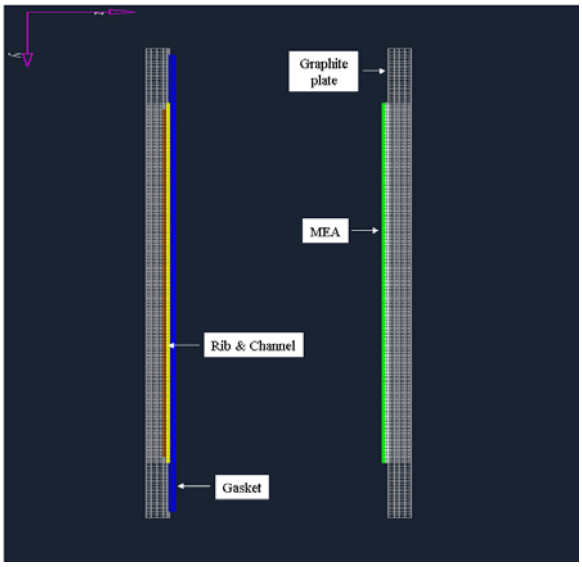
contact pressure distribution between the bipolar plates and the MEA. Thereafter, a further analysis procedure is performed to evaluate the performance of different torques for each of the clamping bolts such that an appropriate contact pressure is obtained between the bipolar plates and the MEA. Note that many commercial single cells and stacks use 2- or 4-bolt clamping designs for time and cost saving of fabrication and assembly. However, no details about their clamping performance are described and understood. Therefore, the other aim of this study is to understand and highlight the possible problems of using the 2- and 4-bolt clamping designs and to compare their performance with that of the 6-bolt clamping design. The example of the selection of 2-, 4- and 6-bolt clamping is to complete the analysis procedures for determining an appropriate clamping to demonstrate the proposed methodology. Overall, the simulation results indicate that the best PEMFC performance is obtained when clamping the two end plates using 6 bolts, each tightened with a torque of 16N-m. It is expected that the bolt number required is dependent on the size and geometry of the fuel cell unit. The larger the fuel cell is, the higher the bolt number is expected. Since the 6-bolt clamping mode with a tightening torque of 16N-m meet the performance requirements of the current fuel cell, the higher-number-bolt clamping are not considered for the time and cost aspects in assembly and manufacture.

3. SIMULATION MODELS

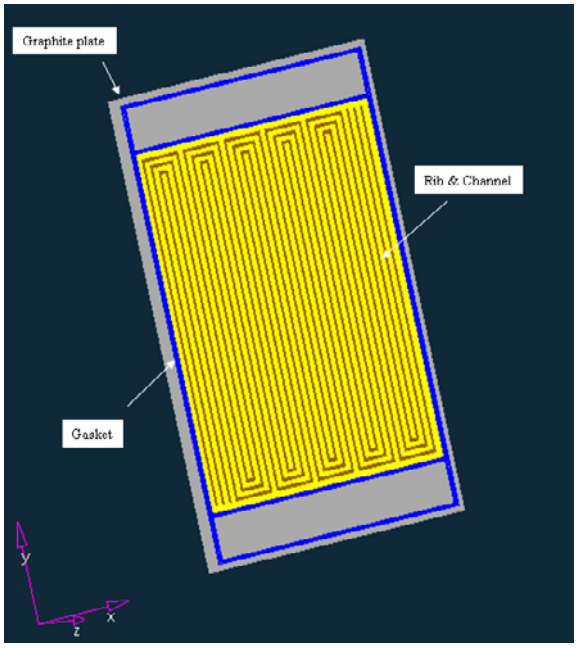
In order to ensure the accuracy of the simulation results, this study constructed a full-size PEMFC model comprised entirely of 3D elements. As shown in Fig. 3, the model contained all of the major components within a typical fuel cell, including the end plates, the bipolar plates, the fluid flow channels, the ribs, the gaskets, the GDLs, the catalyst layers and the proton exchange membrane. In constructing the model, the dimensions and mechanical properties of the various components were specified in accordance with the information available in the published literature. The



(a)



(b)



(c)

Fig. 3 3D finite element models of (a) complete fuel cell; (b) bipolar plate and MEA; (c) interior of graphite bipolar plate with gasket and serpentine fluid channels

https://doi.org/10.1017/jmech.2011.57 Published online by Cambridge University Press

final choice of materials for the gaskets, GDLs and membrane, respectively, was made by performing a series of simulations in which the estimated contact pressure between the bolt head and the end plate of an actual PEMFC was applied to the model and a check was made as to whether the resulting deformations of the PEMFC components remained within the corresponding elastic limits.

The accuracy of the present simulation results depends not only upon constructing a realistic model of the PEMFC, but also upon an appropriate choice of meshing scheme. Due to the complicated geometry of components of the fuel cell and the restrictions of junctions between components (*e.g.* the winding flow channels with small thickness, thin and narrow gaskets, thin membrane/catalyst layer, and their junction problems of elements, *etc*.), it is necessary to mesh the elements to be very small for most components (except parts of end plates). Therefore, we chose first order elements (C3D8 family) for constructing the model. The total element number of the fuel cell model is about 1 million. The meshed elements in our model are small enough to perform accuracy simulations for the purpose of engineering analyses. Furthermore, for the calculation of each case, 16 CPU units in IBM cluster 1350 were used with parallel processes and it took about 25hours. It would take more computational time if the second order element was adopted in the current model. To ensure that there are no errors due to insufficient mesh density or elements with aspect ratios that are too high, mesh independence checks have been performed before analysis. Four mesh numbers, 0.6, 0.8, 1.0 and 1.2 million elements, were tested for the case of 6-bolt clamping arrangement and 6N-m tightening torque. It was found that the simulated differences of the mean contact pressure between models of 0.6 and 0.8 million elements was 15%, between that of 0.8 and 1.0 million elements 6% and between that of 1.0 and 1.2 million elements approximately zero, respectively. Therefore, we chose 1 million elements to mesh the fuel cell model for the analysis. In addition, the aspect ratios of elements for all components, except end plates, are between 1 and 2. For end plates, there are about 28% elements with aspect ratios larger than 2, and the rest of elements equal or less than 2. When checked the meshed model using meshing tool (Altair/HyperMesh software) and performed the simulation using ABAQUS software, no error message was found in the simulation report.

In a previous study, it was shown that for a given compression load, the hydrothermal stress developed within the membrane of a PEMFC is essentially insensitive to the membrane thickness [15]. Furthermore, since the catalytic layers are much thinner than the membrane, their mechanical response under compression need not be considered individually, and thus they can be integrated with the membrane for modeling purposes. Therefore, in constructing the PEMFC model, the total thickness of the membrane / catalyst layer was specified as one fifth that of the GDL. In addition, the elastic modulus of the combined membrane / catalyst layer [18] was assumed to be 10 times higher than that of the GDL [2]. Meanwhile, the anode- and cathode-side bipolar plates were each assumed to contain 3 serpentine fluid channels comprising 63 individual flow paths and occupying a total area of 11.7cm × 8.7cm. The dimensions and mechanical properties of the various components within the final PEMFC model are summarized in Table 1. Note that these dimensions and mechanical properties are similar to those of the fuel cell used in a previous experimental study by the current group [19], and thus the simulation results can be easily verified by way of comparison with the experimental results. It is worth mentioning that the membrane/catalyst layer is very thin. The thickness is 0.1mm and only two-layer elements were meshed. Inside the membrane/catalyst layer, the total number of elements is 40356 and the aspect ratio for all meshed elements is 1. Hence, the differences of simulated results between first order and second order elements are believed to be insignificant, no matter whether it is wet or not. In other words, the simulated deformation and contact pressure should satisfy the analysis demand in the current work, by using first order elements for the model of thin membrane/catalyst layer where the elements are meshed small enough and have a proper aspect ratio.

In the simulations, the effects of the clamping mode on the mechanical response of the PEMFC components were evaluated by predicting the corresponding values of the stress, strain and contact pressure, respectively. In computing the transmitted stresses within the PEMFC, the effects of sliding must be taken into account. Thus, 2D models provide an overly simplistic representation since they assume that all the stress applied to one component is transmitted directly to its neighbor across the interface between them. Conversely, 3D models provide the means to model the stress response over all the contact surface between neighboring elements, and therefore allow both the transmitted stress and the relative sliding phenomenon to be more accurately reproduced. Furthermore, when performing simulations using 2D models, it is generally

Table 1 Dimensions and material properties of components within finite element PEMFC model

Components & Geometry	Length (mm)	Width (mm)	High (mm)	Elastic modulus (MPa)	Poisson's ratio
Bipolar plate	155	95	4	10^4	0.25 [17]
Channel area	117	87			
Channel carved		1.5	0.5		
Rib		1	0.5		
Gasket		1	1	55	0.4 [24]
GDL	117	87	0.5	10	0.25 [2]
Catalyst & Membrane	117	87	0.1	100	0.25 [18]
End plate	250	180	25.6	7×10^4	0.33 (Al)

https://doi.org/10.1017/jmech.2011.57 Published online by Cambridge University Press

necessary to impose a large number of simplifying assumptions, such as a perfect assembly, homogeneous boundary conditions, symmetrical stress and deformation distributions, and so on. As a result, the accuracy of the simulation results can not be guaranteed. Consequently, in this study, the PEMFC model was constructed entirely of 3D solid elements using Altair HyperMesh meshing tool, in which element type of C3D8R was used in constructing most components of the fuel cell and C3D8 was used in the ribs of the flow channels and gaskets, respectively, for a more efficient simulation. To further enhance the accuracy of the simulation results, an assumption was made that each of the PEMFC components was a non-rigid body and therefore deformed non-uniformly when subjected to a compression load. The mechanical responses of the fuel cell components under the effects of the clamping load were evaluated using ABAQUS (Version 6.7-3) finite element analysis (FEA) software. In performing the simulations, the boundary conditions were set with (1) compression force (*i.e.* contact pressure) imposed on the exterior surface nodes of two end plates where bolts and nuts were located and (2) free displacement (*i.e.* zero stress) for the rest of exterior surface nodes of two end plates. Furthermore, the interfacial 3D elements are connected element by element between two adjacent components. However, in a few places, two components that are initially separated by the other component may get into contact after compression. For example, two bipolar plates that are initially separated by the gasket may get into contact after compression. Therefore, in order to avoid the above-mentioned contacted elements after compression pass through each other, the surface-to-surface contact pair feature of the FEA software was set and the friction coefficient between contacted elements was assumed to be 0.1 in the simulation.

4. ANALYSIS METHOD

In general, the compression force acting on the various components within a PEMFC depends on the clamping mode, the geometrical shape of the end plate, and the dimensions and physical properties of the respective components. In this particular study, the aim is to examine the effects of the clamping mode, *i.e.* the clamping torque and the number and arrangement of the clamping bolts, on the performance of the PEMFC. As shown in Fig. 4, the simulations consider three different bolt-clamping modes, namely 2-bolt, 4-bolt and 6-bolt, respectively. In determining the best bolt arrangement among three modes, the factors of interest include the uniformity of the interfacial pressure between the bipolar plates and the GDLs, the contact resistance between the bipolar plates and the MEA, the porosity of the GDLs, and the material strengths of the membrane and gaskets, respectively. Having determined the bolt arrangement, a second series of simulations is performed to establish the proper clamping torque (*i.e.* 6, 8, 12 or 16N-m). Note that prior to analyzing the bolt-clamping mode and clamping torque, respectively, the validity of the

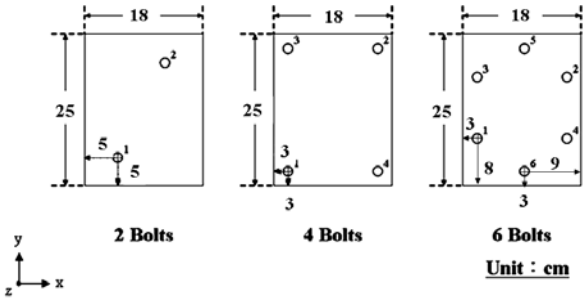


Fig. 4 Three bolt-clamping modes considered in analysis simulations

PEMFC model is verified by performing off-line experiments using a mock- up model of a PEMFC with a pressure-sensitive film embedded between the bipolar plate and the MEA. In the experiments, the pressure acting on the surface of the film is evaluated for each of the three bolt-clamping modes using a default tightening torque of 6N-m. The experimental results are then compared with the corresponding simulation results in terms of both the mean pressure acting on the film and the pixel-by-pixel distribution of the pressure on the film surface.

The electrical performance of a PEMFC is critically dependent upon the contact resistance between the MEA and the bipolar plates, which is governed in turn by the magnitude and uniformity of the clamping force. The literature contains many studies in which the electrical / thermal conduction properties of two contact surfaces are modeled using topography-based theoretical models [20,21]. However, the topographical parameters used in such models are highly complex and difficult to measure. Thus, in this study, the correlation between the pressure at the bipolar plate / GDL interface and the electrical contact resistance is evaluated in accordance with [2]

$$R = \frac{a}{A_c}\left(\frac{b}{P}\right)^{\lambda} \tag{1}$$

where R is the interfacial resistance, A_c is the real contact area, P is the contact pressure and a, b and λ are variables with experimentally determined values. Mishra *et al.* [2] measured the contact resistance between various bipolar plates and GDLs and showed that the interfacial contact resistivity (ρ_s) between a graphite bipolar plate and a carbon paper GDL could be fitted by the analytical formula $\rho_s = a(b/P)^{\lambda}$. Based upon the experimental measurements, the variables a, b and λ were determined to have values of 3.36 (mΩ-cm^2), 1.0 (Mpa) and 0.55, respectively. Accordingly, the same parameter values are used in the present simulations when evaluating the interfacial contact resistance between the bipolar plates and the MEA as a function of the compression force.

In practice, the GDLs in a PEMFC have anisotropic mechanical properties. As a result, the elastic modulus of the GDL in the in-plane direction differs from that in the normal direction. For example, according to the results presented in [2], the in-plane elas-

https://doi.org/10.1017/jmech.2011.57 Published online by Cambridge University Press

tic modulus (E_i) of the GDL is 100MPa, while the cross-plane elastic modulus (E_c) is 10MPa. However, since the fuel cell has a symmetrical structure and the thickness of the GDL is very small compared to its other dimensions, the in-plane deformation of the GDL has a relatively insignificant effect on the contact pressure and bulk strain. Consequently, the simulations performed in this study assume the GDL to be isotropic. In analyzing the clamping mode of the PEMFC, the simulations impose the constraint that each of the components within the fuel cell must remain within its elastic limit. In practice, however, the decision regarding the proper clamping force should be made not only on the basis of the mechanical strength of the PEMFC components, but also upon the effects of the clamping force on the porosity of the GDL since an excessive force may reduce the GDL porosity to such an extent that the migration mechanisms between the anode and cathode sides of the PEMFC are impeded. Assuming the GDL to be fabricated of an elastic, isotropic material, the porosity of the GDL after clamping can be defined as [13]

$$\eta = \frac{V_{\text{empty}}}{V_{\text{total}}} = \frac{\eta_0 - \varepsilon}{1 - \varepsilon} \tag{2}$$

where V_{empty} is the void volume, V_{total} is the total volume of the GDL, η_0 is the initial porosity of the GDL, and $\varepsilon = \varepsilon_{xx} + \varepsilon_{yy} + \varepsilon_{zz}$ is the bulk strain of the GDL.

Note that Eq. (2) is based on the assumption of a small deformation and yields an error of around 5.7% for bulk strains of less than 0.3. Accordingly, in the present simulations, the strain within the GDL is confined to be around the value of 0.3 such that Eq. (2) can be used to analyze the porosity of the GDL as a function of the clamping force. Zhou *et al.* [13] analyzed the efficient gas permeability with liquid water saturation within the porosity ranges from 0.54 to 0.7 for the dry model in which the performance of PEMFC (*i.e.* the current density distribution, the potential losses, the power density, *etc*) induced by different normal clamping pressures were modeled. In their work, the well-known Carman–Kozeny equation was applied to describe the relationships of the porosity and the permeability for both the gas and liquid water phase flows in the two-phase flow model of the cathode. The permeability of both the gas and liquid water phase flows were predicted with the porosity obtained for the dry model only, without knowing the actual porosity in the wet condition. They have shown that the porosity ranging from 0.54 to 0.7 in the dry condition, gives a reasonable range to describe the permeability of a carbon paper. Thus, in the present simulations, the minimum permissible porosity of the GDL following clamping was specified as 0.5. That is, we assigned the porosity of GDL from initial value 0.7 changes to the value of 0.5 after clamping as the range of efficient mass transport process.

To ensure a safe and efficient fuel cell operation, the mechanical strength of the membrane material must be considered over all reasonable values of the temperature, relative humidity, and compression force. When the membrane is compressed as a result of clamping, the most important stress component is that in the normal direction, which has a negative (*i.e.* compressive) value over the entire membrane surface. The transversal stresses are also negative, but are significantly smaller than those in the normal direction. Generally speaking, isotropic membranes are subject to a higher stress following clamping than their anisotropic counterparts [15] Thus, although experimental evidence suggests that the properties of most membrane materials are slightly anisotropic, the present simulations assume the membrane to be isotropic in order to overstate the stress within the membrane slightly so as to introduce a margin of safety into the fuel cell operation.

In traditional engineering practice, the failure of ductile materials is generally analyzed in accordance with one of two different failure criteria, namely the Tresca yield criterion or the von Mises yield criterion, respectively. Of these two criteria, the Tresca yield criterion provides a more conservative estimate of the yield stress. However, the von Mises yield criterion provides a more computationally convenient means of estimating the yield stress in FE analyses since its convenience for the calculation of the normal derivative of the yield function. For an isotropic material, the von Mises yield criterion has the form [22]

$$F(J_2) = J_2 - k^2 = 0\,, \tag{3}$$

where J_2 is an invariant of the stress deviator tensor and k is the yield stress in pure shear. For the elastic limit, Eq. (3) can be re-written in the form of the following stress function:

$$F_0(\sigma_{ij}, k_0) = f(\sigma_{ij}) - k_0^2 = 0\,, \tag{4}$$

where $k_0 = \sigma_0 / \sqrt{3}$ is a material constant, and is determined from uniaxial tension tests; σ_0 is the initial yield stress of the material; and $f(\sigma_{ij})$ is a J_2 function defined as

$$f(\sigma_{ij}) = \frac{1}{2} S_{ij}\, S_{ij}\,, \tag{5}$$

where S is the deviatoric stress tensor and is given by $S_{ij} = \sigma_{ij} - \sigma_m \delta_{ij}$, in which σ_{ij} is the actual stress, $\sigma_m = (1/3)\,\sigma_{ii}$ is the equivalent pressure stress, and δ_{ij} is the Kroneker delta, respectively. The relationship between the von Mises equivalent stress, Q, and the deviatoric stress tensor is expressed as

$$J_2 = \frac{1}{2} S_{ij}\, S_{ij} = \frac{1}{3} Q^2\,. \tag{6}$$

In the present simulations, the proper clamping mode is determined in accordance with the constraint that each of the PEMFC components must remain within its elastic limit when compressed by the clamping force, *i.e.* $F_0(\sigma_{ij}, k_0) = f(\sigma_{ij}) - k_0^2 < 0$.

The literature contains many investigations into the correlation between the mechanical behavior of the membrane and the PEMFC operating conditions.

https://doi.org/10.1017/jmech.2011.57 Published online by Cambridge University Press

Generally speaking, these studies investigate the effects of the temperature or relative humidity on the membrane strength for a fixed compression force [15-17] or consider the effects of the compression force on the mechanical response of the membrane given a constant temperature and relative humidity [14]. Tang *et al*. [18] reported that the elastic modulus and yield stress of a membrane fabricated from Nafion® 112 decreases with an increasing relative humidity and temperature. Therefore, the hydro-thermal conditions of the PEMFC must be taken into account when determining the maximum compressive force which the membrane can withstand following the clamping operation.

As discussed previously, the 3D PEMFC model constructed in this study was certified by performing experimental clamping tests and comparing the experimental measurements for the interfacial contact pressure between the bipolar plate and the MEA with the corresponding simulation results. The experimental PEMFC was constructed using aluminum end plates, graphite bipolar plates, VMQ gaskets, carbon paper GDLs and a Nafion®112 PEM. The dimensions of the various components were identical to those considered in the simulation model except membrane thickness has a slightly difference (see Table 1). Following each clamping test, the interfacial contact pressure was evaluated by disassembling the fuel cell and using a pixel scanner to examine the pressure sensitive film (Ultra Super Low Pressure, FUJI-FILM I&I Imaging & Information) placed between the bipolar plate and the GDL. The accuracy of the FUJI-paper is ±10% or less, according to reference [23].

5. ANALYSIS RESULTS AND DISCUSSIONS

The 3D FE model constructed in this study provides a powerful tool for analyzing the effects of the clamping force on the magnitude and distribution of the interfacial pressure, stress, strain and deformation of each of the components within the PEMFC. As described in Section 3, the model is constructed entirely of 3D solid elements, and thus the simulation results are far more realistic than those obtained using a 2D model. However, the enhanced precision of the simulation results comes at the expense of a significantly higher computational complexity. The FE model comprises somewhere in the region of one million solid elements, and thus a single simulation run designed to model the effects of the clamping force on the mechanical response of the PEMFC components was found to take almost 19hours to complete when performed in parallel on 16 CPUs. Nonetheless, the time and expense incurred in analyzing the PEMFC design and operation using the 3D FE model is significantly less than that which would be incurred if the same process were performed using experimental trial-and-error methods.

Having constructed the FE model, the analysis procedure commenced by considering the effects of the material properties of the gaskets, GDLs and membrane, respectively, on the distribution of the interfacial pressure between the bipolar plate and the MEA. As shown in Table 2, the simulations considered six different combinations of gasket, GDL and membrane materials. Note that the materials assigned to the remaining components within the PEMFC, *e.g.* the end plates and the bipolar plates, remained the same in every case (*i.e.* aluminum and graphite, respectively). The simulation results demonstrated that a more uniform contact pressure was obtained between the bipolar plate and the GDL when the difference between the elastic modulus values of the gasket and membrane, respectively, was reduced. Thus, in performing the remaining simulations, the gasket, GDL and membrane were assumed to be fabricated of VMQ, carbon paper, and Nafion®112, respectively, with the elastic modulus and porosity values shown in the first column of Table 2.

In modeling the effects of the clamping force, the correlation between the tightening torque applied to each bolt and the resulting force acting on the bolt thread transmitted to the end plate was derived in accordance with the formulation [14]

$$F = \frac{2T}{\mu(D_{\text{contact}} + D_{\text{thread}}) + D_{\text{thread}} \tan\alpha} \tag{7}$$

where μ is the friction coefficient, D_{contact} is the average diameter of the contact zone between the head and the end plate, D_{thread} is the diameter of the thread and α is the angle of the thread pitch. In constructing the PEMFC model, it was assumed that the end plates were clamped using M10 bolts, and thus the average diameter and area of the contact region between the bolt head and the end plate were determined to be 9.8mm and 75mm^2, respectively. In addition, the friction coefficient was assumed to have a value of $\mu = 0.2$ (given dry assembly conditions). The force values (and corresponding pressure values) computed using Eq. (7) for the four values of tightening torque considered in the

Table 2 Mechanical properties of alternative materials considered for gasket, GDL and membrane within PEMFC model

Components	Set 1 (E : MPa)	Set 2	Set 3	Set 4	Set 5	Set 6
Gasket	VMQ E = 55 ν = 0.4 [24]	VMQ E = 55 ν = 0.4	Elastomeric E = 200 ν = 0.4 [24]	Elastomeric E = 200 ν = 0.4	Taconic® E = 800 ν = 0.46 [14]	Taconic® E = 800 ν = 0.46
GDL	Carbon paper E = 10 ν = 0.25 Porosity = 0.7 [2]	Same	Same	Same	Same	Same
Membrane	Nafion® 112 E = 100 ν = 0.25 [18]	Nafion membrane E = 190 ν = 0.25 [14]	Nafion® 112 E = 100 ν = 0.25	Nafion membrane E = 190 ν = 0.25	Nafion® 112 E = 100 ν = 0.25	Nafion membrane E = 190 ν = 0.25

https://doi.org/10.1017/jmech.2011.57 Published online by Cambridge University Press

present optimization simulations (namely 6N-m, 8N-m, 12N-m and 16N-m) were 1800N, 2400N, 3600N and 4800N (24N/mm^2, 32N/mm^2, 48N/mm^2 and 64N/mm^2), respectively.

Briefly, as shown in Fig. 2, the analysis process of the methodology comprised three separate sub-procedures. The objective of the first sub-procedure is to verify the validity of the 3D PEMFC model by comparing the simulation results for the interfacial pressure between the bipolar plate and the GDL with the experimental results obtained using a pressure-sensitive film. Meanwhile, the objective of the second sub-procedure is to identify the proper number of clamping bolts, namely the number of bolts which maximizes the uniformity of the contact pressure distribution between the bipolar plate and the GDL. Finally, the objective of the third analysis sub-procedure is to establish the proper clamping torque, *i.e.* the clamping torque which maximizes the compression force between the various components within the PEMFC whilst simultaneously ensuring that the components remain within their elastic limits and the porosity of the GDL has a value of more than 0.5.

According to Tang *et al.* [18], the yield stress of Nafion® 112 reduces from 6.60MPa to 2.29MPa as the temperature and relative humidity are increased from 25°C and 30%, respectively, to 85°C and 90%. Thus, in verifying the performance of the 3D PEMFC model, the target membrane stress was specified initially as 1MPa following the clamping process in order to ensure that the membrane remained well within its operational limit for all realistic hydro-thermal conditions. Simulations were then performed in which the clamping force, F, was progressively increased and the corresponding membrane stress computed. The results showed that the target stress value of 1MPa was obtained using a clamping force of 1800N, corresponding to a clamping torque of 6N-m. Thus, a series of experimental trials was performed in which the PEMFC mock-up model containing a pressure-sensitive film was clamped using 2, 4 and 6 bolts, respectively, with a tightening torque of 6N-m in each case. The experimental results for the interfacial pressure distribution between the bipolar plate and the GDL were then compared with the corresponding simulation results. Figure 5(a) compares the experimental and simulation results for the interfacial pressure contours between the bipolar plate and the GDL given a 6-bolt clamping arrangement and a 6N-m tightening torque. Figure 5(b) presents a statistical analysis of the two sets of pressure results on a pixel (element)-by-pixel (element) basis. From inspection, the mean simulated pressure is determined to be 0.57MPa, while the corresponding experimental value is 0.48MPa. Figure 6 plots the mean simulated and experimental pressure values for clamping arrangements comprising 2, 4 and 6 bolts, respectively. Note that the clamping torque was 6N-m in every case and the experimental values were obtained by averaging the contact pressure of 5 specimens for each clamping bolt mode. Comparing the two profiles in the figure, it is found that the difference between the simulated and experimental pressure values ranges from

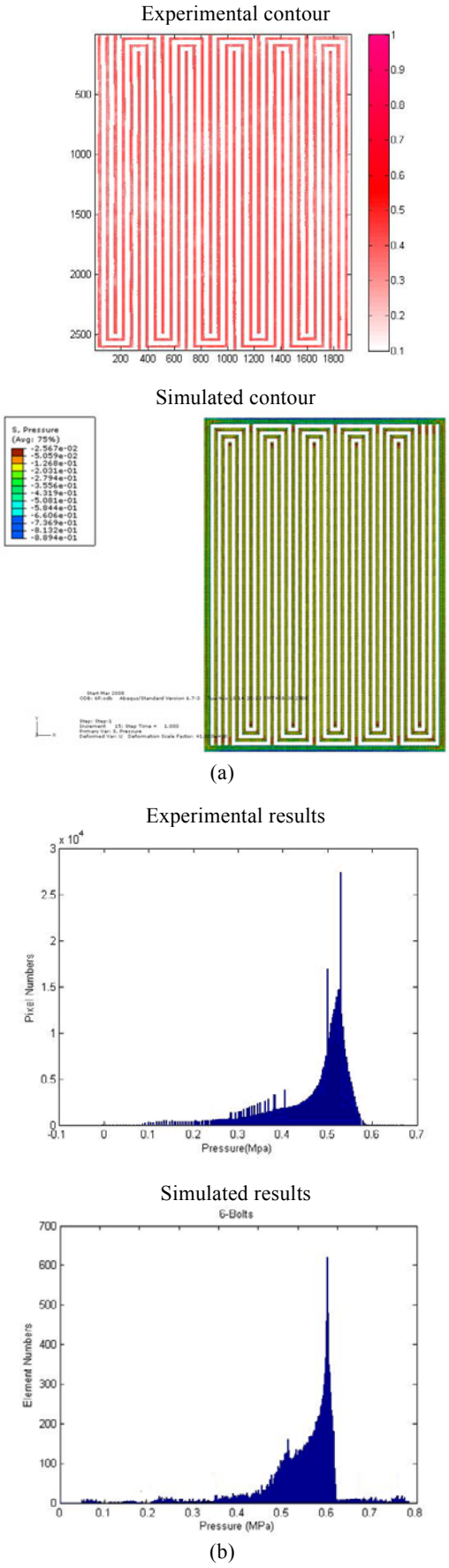


Fig. 5 Experimental and simulations results for (a) pressure contours and (b) contact pressure distribution for 6-bolt clamping mode with 6N-m tightening torque

https://doi.org/10.1017/jmech.2011.57 Published online by Cambridge University Press

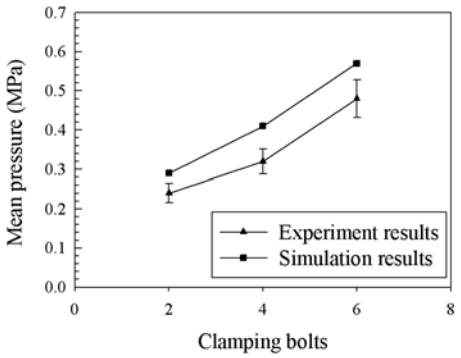
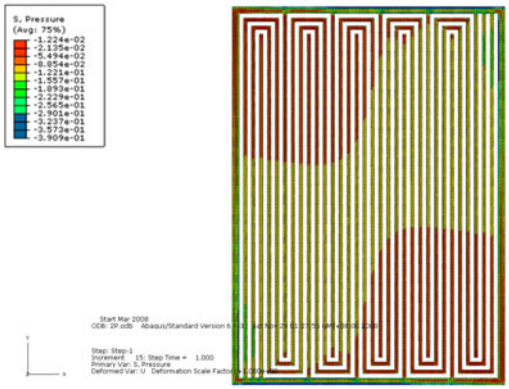


Fig. 6 Experimental and simulation results for variation of mean pressure with number of clamping bolts for a constant tightening torque of 6N-m

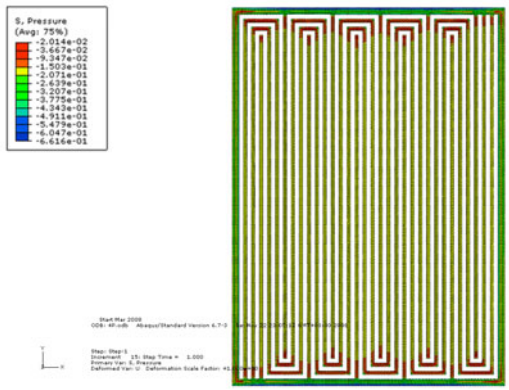
0.05MPa (2-bolt clamping mode) to 0.09MPa (6-bolt clamping mode), corresponding to an error range of 17 ~ 22%. These error values are relatively small compared with those presented by Lee *et al*. [11], and thus the validity of the 3D PEMFC model is confirmed.

Having confirmed the suitability of the 3D PEMFC model for simulation purposes, a series of simulations was performed to establish the optimal bolt-clamping mode, *i.e.* 2-bolt, 4-bolt or 6-bolt. As shown in the second sub-procedure in Fig. 2, the simulations assumed a clamping torque of 6 N-m in every case in order to ensure that the membrane stress did not exceed the specified value of 1MPa. In performing the simulations, the objective was to establish the bolt-clamping mode which maximized the uniformity of the pressure distribution between the bipolar plate and the GDL. Figures 7(a) ~ (c) present the simulated interfacial pressure contours for the 2-bolt, 4-bolt and 6-bolt clamping modes, respectively. The corresponding statistical analysis results are presented in Fig. 8. Overall, the figures show that the 2-bolt clamping mode results in the lowest interfacial pressure and the most non-uniform distribution of the contact pressure. By contrast, the 4-bolt and 6-bolt clamping modes produce a higher interfacial pressure and a more uniform pressure distribution. Figures 9 and 10 present the simulation results obtained for the deformation distributions of the bipolar plate and GDL, respectively, under the 4-bolt clamping mode (Figs. 9(a) and 10(a)) and the 6-bolt clamping mode (Figs. 9(b) and 10(b)). It is observed that the 4-bolt clamping mode produces regions of significant deformation in the central parts of both the bipolar plate and the GDL. On the other hand, the 6-bolt clamping mode yields more uniformly distribution of the deformation over the entire surface areas of the bipolar plate and GDL than that of the 4-bolt clamping mode. Thus, overall, the results presented in Figs. 7 ~ 10 indicate that the 6-bolt clamping mode (see rightmost schematic in Fig. 4) represents the ideal clamping mode for the PEMFC since it maximizes both the magnitude and the uniformity of the interfacial pressure between the bipolar plate and the GDL.

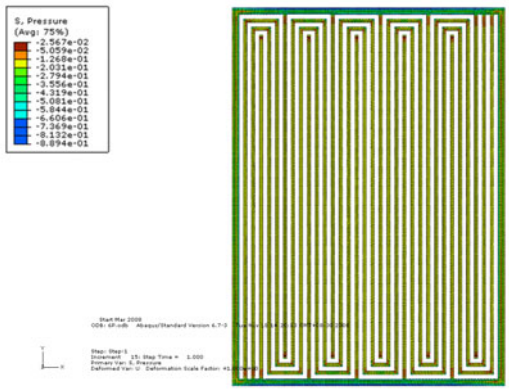
Having determined the proper bolt-clamping mode, a further series of simulations was performed to determine the proper tightening torque. As the final (third)



(a) 2 Bolts



(b) 4 Bolts

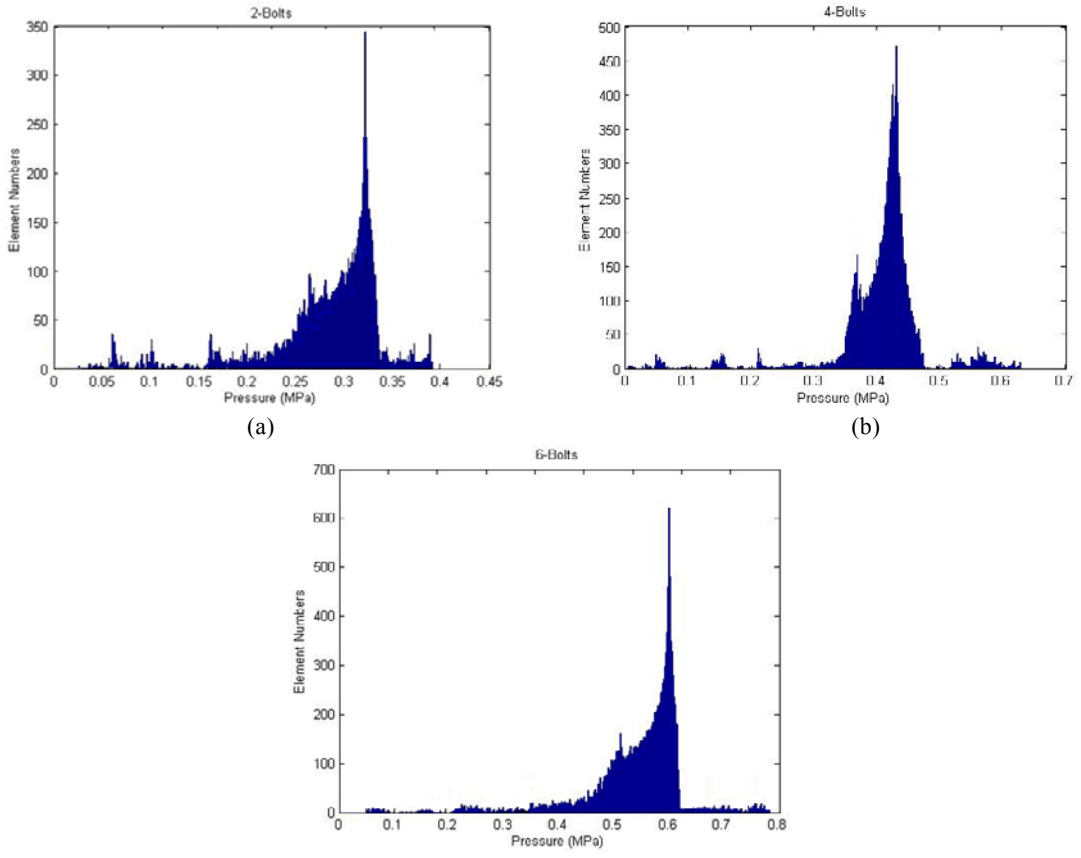


(c) 6 Bolts

Fig. 7 Simulation results for interfacial contact pressure contours between bipolar plate and GDL for (a) 2-bolt; (b) 4-bolt; and (c) 6-bolt clamping modes

sub-procedure shown in Fig. 2, the simulations commenced by assigning a clamping torque of 6N-m to each of the 6 bolts in the end plate. The values of six parameters of interest were then derived, namely the maximum membrane stress, the maximum gasket stress, the average GDL strain, the average GDL porosity, the average interfacial contact pressure and the electrical contact resistance. The simulation procedure was then repeated for clamping torques of 8N-m, 12N-m and 16N-m, respectively. The objective of the simulations was to determine the tightening torque which maximized the interfacial pressure between the bipolar plate and the GDL whilst simultaneously ensuring that the

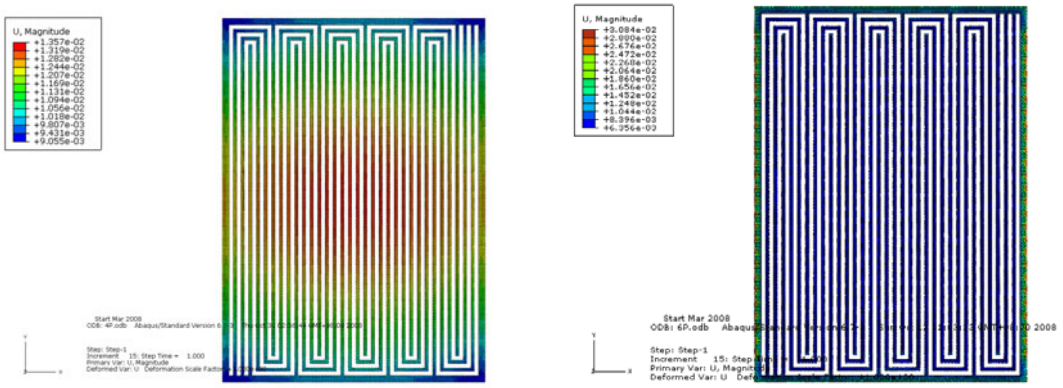
https://doi.org/10.1017/jmech.2011.57 Published online by Cambridge University Press



(a) (b)

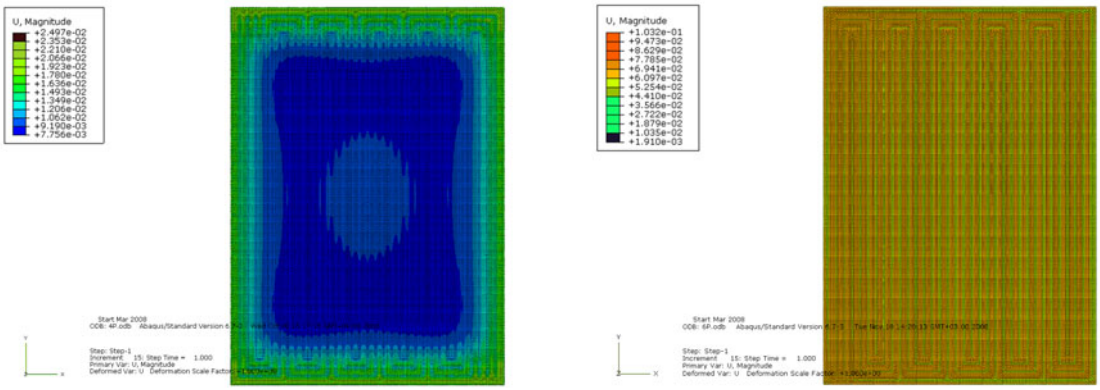
(c)

Fig. 8 Statistical analysis results for contact pressure distributions shown in Figs. 7(a) ~ (c)



(a) (b)

Fig. 9 Simulation results for distribution of bipolar plate deformation for: (a) 4-bolt, and (b) 6-bolt clamping modes



(a) (b)

Fig. 10 Simulation results for distribution of GDL deformation for: (a) 4-bolt, and (b) 6-bolt clamping modes

https://doi.org/10.1017/jmech.2011.57 Published online by Cambridge University Press

membrane and gaskets remained within their respective elastic limits and the porosity of the GDL has a value higher than 0.5. Note that in performing the simulations, the hydro-thermal conditions of the PEMFC were specified as room temperature (*i.e.* 25°C) and a membrane moisture content of 50%, respectively. In practice, the yield strength of a PEMFC membrane depends on both the temperature and the relative humidity. Also, determining the precise value of the membrane yield strength for any particular set of hydro-thermal conditions is difficult. However, according to the results presented by Tang *et al.* [18], the breaking stress of the Nafion® 112 membrane considered in the current 3D PEMFC model reduces from 17MPa at a temperature of 25°C and a relative humidity of 30% to 9MPa for a temperature and relative humidity of 85°C and 90%, respectively. Furthermore, in [18], it was shown that the yield strength of a Nafion® 112 membrane in simple tension was 6.14MPa for the hydro-thermal conditions considered in the present simulations (namely a temperature of 25°C and a membrane moisture content of 50%). From Eq. (4), the corresponding yield stress is determined to be 5.9MPa. Thus, in performing the simulations, the maximum permissible value of the membrane stress was specified as 5.9MPa. The yield stress of the VMQ (silicone rubber) gaskets within the PEMFC model also varies with the hydro-thermal conditions. Thus, in the present simulations, the maximum permissible value of the gasket stress was specified as 50MPa in accordance with the yield strength data presented in [25]. The simulation results obtained for each of the six parameters of interest are summarized in Table 3 for each value of the tightening torque. From inspection, the best tightening torque is determined to be 16N-m, corresponding to a maximum membrane stress (out-of-plane normal stress) of 5.62MPa, a maximum gasket stress (out-of-plane normal stress) of 16.9MPa and a GDL porosity of 0.545.

In verifying the validity of the numerical model and determining the proper number of clamping bolts, the distribution of the interfacial pressure between the bipolar plate and the GDL was evaluated by means of pressure contour plots and a pixel (element)-by-pixel (element) statistical analysis technique (see Figs. 5, 7 and 8). However, a more quantitative evaluation of the interfacial pressure distribution can be obtained using the following dimensionless pressure disturbance parameter [24]:

$$P_H = \frac{P'}{\overline{P}} \tag{8}$$

where P' is the standard deviation of the simulated pressure values over the contact surface between the bipolar plate and the GDL, and $\overline{P}$ is the mean pressure. Basically, P_H indicates the degree of uniformity of the pressure distribution, with a lower value implying a more uniform distribution. In Eq. (8), the standard deviation of the pressure is defined as

$$P' = \sqrt{\frac{1}{N-1}\sum_{i=1}^{N}(P_i - \overline{P})^2} \tag{9}$$

Table 3 Values of major parameters of interest for clamping torques in the range 6 ~ 16N-m

T (N-mm)	σ, Max (Membrane, MPa)	σ, Max (Gasket, MPa)	ε_B, Ave (GDL)	η, Ave (GDL)	P, Ave (Contact pressure, MPa)	R (Contact resistance, mΩ)
6×10^3	2.11	5.8	0.11	0.661	0.57	0.09
8×10^3	2.81	7.9	0.147	0.645	0.77	0.07
12×10^3	4.21	12.2	0.228	0.604	1.22	0.057
16×10^3	**5.62**	**16.9**	**0.315**	**0.545**	**1.68**	**0.05**

where N denotes the total number of 3D elements in the interfacial contact area between the bipolar plate and the GDL and P_i is the pressure acting on element i. Similarly, the uniformity of the GDL porosity distribution can be quantified by replacing the terms P' and $\overline{P}$ in Eq. (8) by η' and $\overline{\eta}$, respectively, to give a dimensionless porosity disturbance parameter η_H. Taking the simulation results for the pressure distribution and porosity distribution as input data, the corresponding values of the dimensionless pressure and porosity disturbance parameters can be easily obtained using a simple MATLAB computer program. Note that the local porosity of the GDL is evaluated using Eq. (2) based on the element bulk strain of the GDL.

Figure 11 shows the variation of the mean contact pressure between the bipolar plate and the GDL with the clamping torque for each of the three bolt-clamping modes. The results clearly show that the magnitude of the mean interfacial pressure increases with both an increasing clamping torque and an increasing number of clamping bolts. Figure 12 illustrates the effect of the clamping torque and the bolt-clamping mode on the electrical contact resistance between the bipolar plate and the GDL. Note that in using Eq. (1) to calculate the electrical contact resistance from the simulated values of the mean pressure, an assumption was made that the bipolar plate and GDL make perfect contact, and thus the term A_c in Eq. (1), *i.e.* the real contact area, was set equal to the theoretical contact area, *i.e.* 11.7cm × 8.7cm = 101.79cm^2. The results show that in the 6-bolt clamping mode, the contact resistance reduces from 0.09mΩ to 0.05mΩ as the clamping torque is increased from 6N-m to 16N-m. Figure 13 illustrates the variation of the pressure disturbance parameter P_H with the clamping torque for the 2-bolt, 4-bolt and 6-bolt clamping modes, respectively. The results confirm that the 6-bolt clamping mode not only yields a more uniform pressure distribution than the 2- or 4-bolt clamping modes for any given value of the clamping torque, but also provides a more rapid improvement in the uniformity of the pressure distribution as the value of the clamping torque is increased. Figure 14 plots the variation of the dimensionless porosity disturbance parameter η_H with the clamping torque for each of the three bolt-clamping modes. As expected, the uniformity of the porosity distribution increases with an increasing clamping torque. However, comparing the

https://doi.org/10.1017/jmech.2011.57 Published online by Cambridge University Press

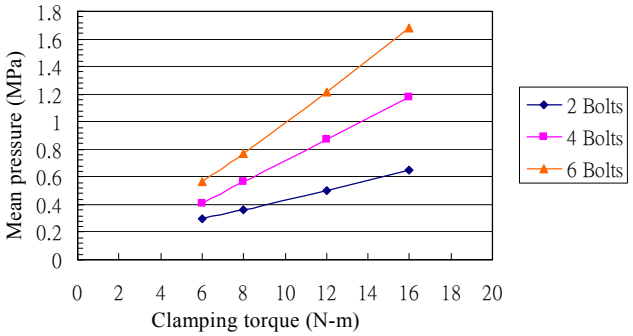


Fig. 11 Variation of mean contact pressure between bipolar plate and GDL with clamping torque for different bolt clamping modes

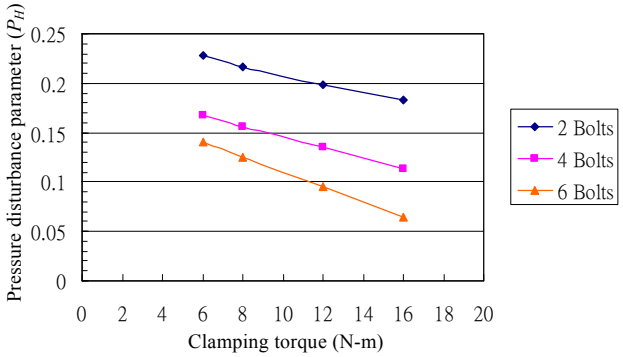


Fig. 13 Variation of dimensionless pressure disturbance parameter with clamping torque for different bolt clamping modes

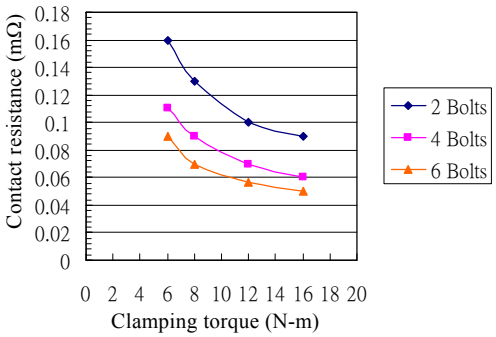


Fig. 12 Variation of contact resistance between bipolar plate and GDL with clamping torque for different bolt clamping modes

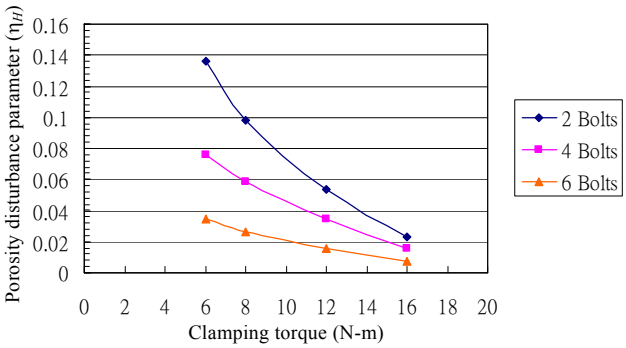


Fig. 14 Variation of porosity disturbance parameter with clamping torque for different bolt clamping modes

results presented in Figs. 13 and 14, it is seen that while the pressure disturbance parameter reduces linearly with an increasing clamping torque, the porosity disturbance parameter decreases non-linearly. Figure 15 illustrates the effect of the clamping torque and bolt-clamping mode on the mean porosity of the GDL as evaluated using Eq. (2) based on the mean bulk strain of the GDL. Comparing the results presented in Figs. 14 and 15, it is evident that the uniformity of the GDL porosity distribution tends to improve as the porosity of the GDL reduces. Consequently, the 6-bolt clamping mode uniformizes the GDL porosity distribution, but results in the lowest GDL porosity due to the correspondingly higher value of the clamping force. However, in practice, the loss in porosity is more than compensated for by the better uniformity of the porosity distribution, which improves the efficiency of the fluid transfer through the GDL and reduces the contact resistance.

Two points are worth addressing: (1) In the current bolt-clamping modes shown in Fig. 4, the positioning of the 4-bolt clamping mode is worse than the 6-bolt clamping mode, because the 4-bolt set is positioned more at the outside than the 6-bolt set (relative to the bipolar plates and MEA). Therefore, the direct comparison between the results of 4-bolt and 6-bolt clamping modes may not be appropriate (bolt-positionwise). However, the general methodology for analyzing the clamping of PEMFC and conclusions obtained under the current designed clamping modes are still justified; (2) for a practical fuel cell system, there would be a maximum power density if an optimal clamping force is found. The optimal design parameters for a real fuel cell system depends on the mechanical and electrical properties of the bipolar plates and gas diffusion layer, and the interfacial electrical property and the across shape of the bipolar plates, *etc*. This work deals with analysis of proper clamping mode with consideration of only mechanical properties such as the mean interfacial contact pressure between the bipolar plate and the GDL and its uniformity, the deformation of the bipolar plate, the deformation of the GDL, the contact resistance between the bipolar plate and the GDL, and the porosity of the GDL, *etc*. The simulation results demonstrated that for the assigned hydro-thermal conditions (*i.e.* a temperature of 25°C and a membrane moisture content of 50%), the clamping configuration (6-bolt and 16N-m) ensures the lowest contact resistance, with the porosity of the GDL higher than 0.5 in order to maximize the efficiency of the mass transport process and the membrane and gaskets remained within their elastic limits in order to ensure the mechanical integrity of the fuel cell. As the fuel cell is in operation, more factors such as water contained in the porous membrane, swelling of porous layers, electron/fuel/water transport, temperature effect, *etc*., are involved. In this situation, the coupling effects of clamping force and hydro-thermal conditions on the electrical performance of the PEMFC (*e.g.* the power, current density, output voltage, and so on) need to be investigated in detail, with the combined efforts of finite element method described in this work

https://doi.org/10.1017/jmech.2011.57 Published online by Cambridge University Press

and CFD (computational fluid dynamics) method to consider the elastic deformation of the GDL and the mass transport of the reactants and products together. However, the analysis procedure still provides a useful tool for the PEMFC clamping design before the real implementation.

6. CONCLUSION

This study emphasizes the development of an analysis method for the proper clamping design of a PEMFC. The aim was two-fold, namely (1) to ensure a uniform distribution of the interfacial pressure between the bipolar plates and the GDLs in order to enhance the efficiency of the fuel cell, and (2) to maximize the interfacial pressure between the bipolar plates and the MEA in order to minimize the electrical contact resistance. Taking the traditional and most popular point-load design with the assembly of several pairs of bolts and nuts as the example, this study has constructed a full-scale 3D finite element model of a PEMFC comprising virtually all of the components within a real-world fuel cell. The constructed model provides a powerful tool for optimizing the PEMFC design and operation for the performed example cases without the need for physical experimentation. Generally, in the proposed methodology, a systematic approach was applied to analyze the PEMFC clamping mode, *i.e.* the number of clamping bolts and the tightening torque. The analysis procedure was performed subject to two constraints, namely (1) to ensure that the membrane and gaskets remained within their elastic limits in order to ensure the mechanical integrity of the fuel cell, and (2) to ensure that the porosity of the GDL has a value higher than 0.5 in order to maximize the efficiency of the mass transport process. Overall, the simulation results demonstrated that for the assigned hydro-thermal conditions (*i.e.* a temperature of 25°C and a membrane moisture content of 50%), the optimal fuel cell performance was obtained using a 6-bolt clamping mode, with each bolt tightened to a torque of 16N-m, among the performed examples.

The simulation results presented in this study provide a useful insight into the effects of the clamping mode on the contact resistance between the bipolar plates and the MEA and the mechanical response of the various PEMFC components, respectively. Although the proposed analysis method was applied to a single fuel cell with different bolt configurations in the study (point-load design), the proposed systematically approach should be applicable to the optimization of other clamping methods, including line-load design and surface-load design.

ACKNOWLEDGMENTS

The present study was supported by the National Science Council, Taiwan, the Republic of China, through the grant numbers NSC 97-2622-E-006-028-CC. Authors are also grateful to the National Center for High Performance Computing, Taiwan, for providing the computational resources.

LIST OF SYMBOLS

Latin letters

A_c	real contact area at the bipolar plate / GDL interface
D_{contact}	average diameter of the contact zone between bolt head and end plate
D_{thread}	diameter of thread of the bolt
E_c	cross-plane elastic modulus of the GDL
E_i	in-plane elastic modulus of the GDL
F	clamping force
J_2	invariant of the stress deviator tensor
k	yield stress in pure shear
N	total number of 3D elements in the interfacial contact area between bipolar plate and GDL
P	contact pressure at the bipolar plate / GDL interface
P_i	the pressure acting on element i
P_H	dimensionless pressure disturbance parameter
P'	standard deviation of pressure values over the contact surface between bipolar plate and GDL
$\overline{P}$	mean pressure of the contact surface between bipolar plate and GDL
Q	von Mises equivalent stress
S_{ij}	deviatoric stress tensor
T	tightening torque
V_{empty}	void volume of the GDL
V_{total}	total volume of the GDL
R	interfacial resistance between graphite plate and GDL

Greek letters

a	angle of the thread pitch
δ_{ij}	Kroneker delta
ε	bulk strain of the GDL
η	porosity of the GDL after clamping
η_0	initial porosity of the GDL
η_H	dimensionless porosity disturbance parameter
μ	friction coefficient
ρ_s	interfacial contact resistivity
σ_0	initial yield stress of the material
σ_{ij}	actual stress of interface
σ_m	equivalent pressure stress

REFERENCES

1. Lee, W. K., Ho, C. H., Zee, J. W. V. and Murthy, M., "The Effects of Compression and Gas Diffusion Layers on the Performance of a PEM Fuel Cell," *Journal of Power Sources*, **84**, pp. 45–51 (1999).

https://doi.org/10.1017/jmech.2011.57 Published online by Cambridge University Press

2. Mishra, V., Yang, F. and Pitchumani, R., "Measurement and Prediction of Electrical Contact Resistance Between Gas Diffusion Layers and Bipolar Plate for Applications to PEM Fuel Cells," *Journal of Fuel Cell Science and Technology*, ASME, **1**, pp. 2–9 (2004).
3. Wang, H., Sweikart, M. A. and Turner, J. A., "Stainless Steel as Bipolar Plate Material for Polymer Electrolyte Membrane Fuel Cells," *Journal of Power Sources*, **115**, pp. 243–251 (2003).
4. Tian, R., Sun, J. and Wang, L., "Plasma-Nitrided Austenitic Stainless Steel 316L as Bipolar Plate for PEMFC," *International Journal of Hydrogen Energy*, **31**, pp. 1874–1878 (2006).
5. Zhan, Z., Xiao, J., Zhang, Y., Pan, M. and Yuan, R., "Gas Diffusion Through Differently Structured Gas Diffusion Layers of PEM Fuel Cells," *International Journal of Hydrogen Energy*, **32**, pp. 4443–4451 (2007).
6. Dohle, H., Jung, R., Kimiaie, N., Mergel, J. and Muller, M., "Interaction Between the Diffusion Layer and the Flow Field of Polymer Electrolyte Fuel Cells—Experiments and Simulation Studies," *Journal of Power Sources*, **124**, pp. 371–384 (2003).
7. Pharoah, J. G., "On the Permeability of Gas Diffusion Media Used in PEM Fuel Cells," *Journal of Power Sources*, **144**, pp. 77–82 (2005).
8. Chu, D. and Jiang, R., "Performance of Polymer Electrolyte Membrane Fuel Cell (PEMFC) Stacks: Part I. Evaluation and Simulation of an Air-Breathing PEMFC Stack," *Journal of Power Sources*, **83**, pp. 128–133 (1999).
9. Jiang, R. and Chu, D., "Stack Design and Performance of Polymer Electrolyte Membrane Fuel Cells," *Journal of Power Sources*, **93**, pp. 25–31 (2001).
10. Giddey, S., Ciacchi, F. T. and Badwal, S. P. S., "Design, Assembly and Operation of Polymer Electrolyte Membrane Fuel Cell Stacks to 1 Kwe Capacity," *Journal of Power Sources*, **125**, pp. 155–165 (2004).
11. Lee, S. J., Hsu, C. D. and Huang, C. H., "Analyses of the Fuel Cell Stack Assembly Pressure," *Journal of Power Sources*, **145**, pp. 353–361 (2005).
12. Zhou, P., Wu, C. W. and Ma, G. J., "Contact Resistance Prediction and Structure Optimization of Bipolar Plates," *Journal of Power Sources*, **159**, pp. 1115–1122 (2006).
13. Zhou, P., Wu, C. W. and Ma, G. J., "Influence of Clamping Force on the Performance of PEMFCs," *Journal of Power Sources*, **163**, pp. 874–881 (2007).
14. Bograchev, D., Gueguen, M., Grandidier, J. C. and Martemianov, S., "Stress and Plastic Deformation of MEA in Fuel Cells: Stresses Generated During Cell Assembly," *Journal of Power Sources*, **180**, pp. 393–401 (2008).
15. Tang, Y., Santare, M. H. and Karlsson, A. M., "Stress in Proton Exchange Membranes Due to Hygro-Thermal Loading," *Journal of Fuel Cell Science and Technology*, ASME, **3**, pp. 119–124 (2006).
16. Kusoglu, A., Karlsson, A. M., Santare, M. H., Cleghorn, S. and Johnson, W. B., "Mechanical Response of Fuel Cell Membranes Subjected to a Hygro-Thermal Cycle," *Journal of Power Sources*, **161**, pp. 987–996 (2006).
17. Kusoglu, A., Karlsson, A. M., Santare, M. H., Cleghorn, S. and Johnson, W. B., "Mechanical Behavior of Fuel Cell Membranes Under Humidity Cycles and Effect of Swelling Anisotropy on the Fatigue Stresses," *Journal of Power Sources*, **170**, pp. 345–358 (2007).
18. Tang, Y., Karlsson, A. M., Santare, M. H., Gilbert, M., Cleghorn, S. and Johnson, W. B., "An Experimental Investigation of Humidity and Temperature Effects on the Mechanical Properties of Perfluorosulfonic Acid Membrane," *Journal of Material Science and Engineering A*, **425**, pp. 297–304 (2006).
19. Wen, C. Y., Lin, Y. S. and Lu, C. H., "Performance of a Proton Exchange Membrane Fuel Cell Stack with Thermally Conductive Pyrolytic Graphite Sheets for Thermal Management," *Journal of Power Sources*, **189**, pp. 1100–1105 (2009).
20. Majumdar, A. and Tien, C. L., "Fractal Network Model for Contact Conductance," *Jt. ASME/AIChE National Heat Transfer Conference*, Philadelphia, PA, pp. 1–9 (1989).
21. Majumdar, A. and Tien, C. L., "Fractal Network Model for Contact Conductance," *Journal of Heat Transfer*, **113**, pp. 516–525 (1991).
22. Chen, W. F. and Han, D. J., Plasticity for Structural Engineers, Gau Lih Book Co., LTD. Taiwan, (1995).
23. http://www.fujifilm.com/, December (2009).
24. Wen, C. Y., Lin, Y. S. and Lu, C. H., "Experimental Study of Clamping Effects on the Performances of a Single Proton Exchange Membrane Fuel Cell and a Ten-cell Stack," *Journal of Power Sources*, **192**, pp. 475–485 (2009).
25. International lubricant Standardization and Approval Committee, January 23, Draft: 8, (2008).

(Manuscript received April 28, 2010,
accepted for publication January 5, 2011.)

https://doi.org/10.1017/jmech.2011.57 Published online by Cambridge University Press